International Journal of Steel Structures (2019) 19(4):1302–1316
https://doi.org/10.1007/s13296-019-00211-9

Online ISSN 2093-6311
Print ISSN 1598-2351

Effect of Shear and Distortion Deformations on Lateral Buckling Resistance of Box Elements in the Framework of Eurocode 3

Abdelkader Saoula[1] · **Sid Ahmed Meftah**[1]

Received: 29 March 2018 / Accepted: 29 January 2019 / Published online: 4 March 2019

Abstract
This paper treats the distortional and shear deformation effects on the elastic lateral torsional buckling of thin-walled box beam elements, under combined bending and axial forces. For the purpose, a nonlinear kinematic model based on higher order theory is used applicable to both short and long thin-walled box beams. Because in the kinematic model of the higher order theory integrates additional flexibility terms related to shear, distortion and warping effects, it accurately predicts the lateral torsional buckling of the straight box beams. Ritz's method is adopted as solution strategy in order to obtain the nonlinear governing equilibrium equations, then the buckling loads are computed by solving the eigenvalue problem basing on the singularity of the tangential stiffness matrix. Owing to flexural–torsional and distortional couplings, new matrices are obtained in both geometric and initial stress parts of the tangent stiffness matrix. The proposed method with the new stiffness terms, is efficient and accurate in lateral torsional buckling predictions, when compared with the commercial FEM code ABAQUS results. Based on the existing European guidelines EC3, an extensive numerical investigation is performed to demonstrate the effects of both shear and distortional deformations on the moment carrying capacity. The convenience of the model is outlined and the limit of models developed without shear and distortion deformation effects on lateral buckling loads evaluation is discussed.

Keywords Non-linear · Lateral-Torsional Buckling · Box beams · Ritz's method · Distortion and shear deformations · Eurocode 3

1 Introduction

Steel box beams are very frequently incorporated into high rise buildings as an efficient means for providing resistance to lateral forces arising from winds and strong ground motions. The box beams are also commonly used in plane frames for pipe supports, industrial structures in power plants, oil refineries, and petro-chemical industrial plants.

When designing these structures (box beams), it is important to quantify their lateral torsional buckling resistance under in-plane loads. This resistance can be achieved by adopting a one-dimensional beam buckling element with shear and distortion degrees of freedom.

Following the Eurocode 3 (Eurocode 1992), LTB for rectangular hollow section need not to be checked. This is due to the fact that their polar moment of inertia is very large and therefore the section is more vulnerable to local instability phenomena. This statement may be explained by the fact that Eurocode 3 rules are restricted to steel grades for which the yield strength, $f_y \leq 265$ MPa. However, with the recent development of high strength steels ($f_y > 700$ MPa), the buckling strength of the box beam cannot be predicted through simplified code procedures, which neglect shear and distortion deformations. Instead the analyst could resort to shell finite element analysis; a viable but impractical option in typical design environments.

Additional guidelines for box cross section beams where the lateral buckling are described in Rondal et al. (1992). It was found from this report that, the adopted solutions are similar to the ones of classical thin-walled beams having open sections. They are derived from the linear stability theory, when the distortional and shear deformations are omitted.

Recently Saoula et al. (2016) have presented a simplified analytical model for more accurate LTB prediction of doubly supported beam under combined axial and bending loads. The authors have developed a powerful analytical method

✉ Sid Ahmed Meftah
meftahs@yahoo.com

[1] Laboratoire des Structures et Matériaux Avancés dans le Génie Civil et Travaux Publics, Université de Djillali Liabes, Sidi Bel Abbes, Algérie

for elastic lateral torsional buckling resistance for simply supported rectangular box beams. Regard to this model, the distortional deformation effect on LTB results have been considered. It has been demonstrated that when the stability of long beams are investigated, the shear deformation effects are not important for simple supported beam and the model leads to close buckling moments. However, the accuracy loss by this model cannot be avoided in the cases of cantilever short beams due to the shear forces contribution in the beam stiffness. They therefore provide an additional link between bending shear and distorsion deformations.

Within this context, the current study develops a simplified one-dimensional beam buckling element under combined bending and axial forces. The displacements field of the proposed element are affected by additional degrees of freedom representing transverse shear and distortion deformations. In the kinematical model finite torsion assumption has been admitted. This assumption is admitted when the stability of rectangular box beams with width to height ratio less than 0.5 are investigated.

Based on Ritz's method, the governing equilibrium equations of a box beam are obtained. These ones are nonlinear and strongly coupled. This model provides the lateral buckling resistance by requiring the singularity condition of the tangent stiffness matrix.

The objectives of this study are: (a) to present an improved analytical solution able to analyze the elastic LTB behavior of cantilever steel box beams under combined compressive and bending loads; (b) to provide the incidence of the obtained result of the LTB on the moment carrying capacity; and (c) to illustrate the influence of the yield stress on the moment carrying capacity given by the proposed approach.

2 Literature Review

Past researches on box beams considering distortion deformation are focused only on static and free vibrations problems by adopting linear kinematic models. For these kinds of problems, the literature is rich in theories and numerical models.

A 3D model was employed to provide an exact solution capable of predicting the cross-section distortion (Hughes 1983; Bull 1988). In the case of beams with small aspect ratio an improved analytical method was proposed (Boitzov 1972; Boswell and Zhang 1984; Boswell and Li 1995; Hsu et al. 1995; Pavazza and Matokovic 2000; Pavazza 2002).

Balch (1986) and Balch and Steele (1987) have addressed the significant local influences related to sectional distorsion of thin-walled closed beam. Kim and Kim (1999, 2000, 2002) have proposed a new one dimensional theory for static and dynamic analysis of thin-walled closed beam.

Recently, more improved higher-order beam theories dedicated to the box beam joint systems have been proposed by Gang-won et al. (2013) and Choi and Kim (2016a, b).

A large number of research papers concerned with the buckling of compressed rectangular box beams are available in the literature for example by Jombock and Clark (1961), Graves Smith (1967, 1971), Svenson and Croll (1975), Skaloud and Naprstek (1977), Braham et al. (1980) and Rhodes (2002) among many others.

Design specifications related to tubular members are available throughout the world, and research on tubular sections in materials such as stainless steel (Rasmussen 2000), or tubular sections filled with various materials such as concrete (Zhao and Grzebieta 2000), wood or polyurethene foam (Gupta et al. 2000) has been widely reported.

Kim and Yoo (2008) have examined the ultimate strength interaction between bending and torsion for built-up steel rectangular box beams by a nonlinear incremental Finite Element Method (FEM) using the commercial program, ABAQUS (2003).

Although some papers are focused on the LTB of steel thin-walled beams with open sections (Benyamina et al. 2013; Mohri et al. 2015; Asgarian et al. 2013) scant works are available in the case of steel box beam structures (Saoula et al. 2016). For such structures, analysts and designers are compelled to resort to the rules and recommendations of design codes and standards, namely American Institute of Steel Construction (AISC 1994) and European Steel Code (Eurocode 3 1992).

3 Equilibrium Equations for Buckling Analysis

3.1 Kinematics

One considers a straight thin-walled box beam of length L as shown in Fig. 1. The width and height of the beam are denoted by b and h respectively and wall thickness by$t$.

In the case of a thin-walled box beam considered here, one describes the shell displacements of a point on the contour in terms of the axial $u^i(s,x,n)$, tangential $v^i(s,x,n)$ and normal $w^i(s,x,n)(i=1.0.4)$ components as pictured in Fig. 2. These displacements are referenced to a curvilinear coordinate system attached to each wall unit. The tangential coordinate s is measured counter-clockwise along the tangent to the middle surface, while the normal coordinate n directs outwards from the surfaces as indicated in Fig. 2. Additionally to the mentioned local coordinate system (s,x,n), a direct global coordinate system x, y *and* z is reported to represent the sectional deformation of a thin-walled beam by using a one-dimensional theory. The origin of this referential is located at the centroid G. Since the study concerns the bi-symmetrical shape section beams, the shear centre C coincides with the centroid G.

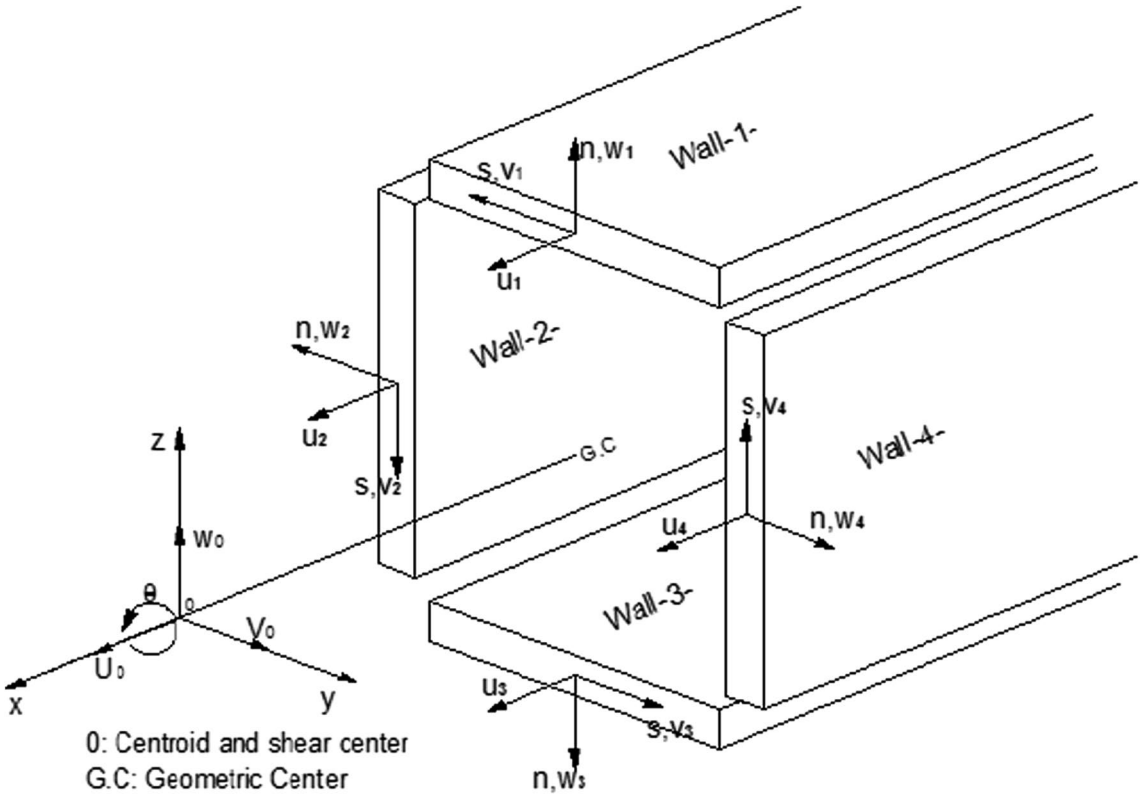

Fig. 1 The local coordinate system, the origin is located at the centre of each wall

Unlike the conventional thin-walled theory (Benyamina et al. 2013; Mohri et al. 2015; Asgarian et al. 2013) for open sections, the beams with closed cross sections are shown to exhibit significant distortional deformations. Also, in this study, we are mainly concerned with the beams that possess large bending and torsion stiffness. Under these conditions, he wall 3D displacements are expressed as follows:

$$u^i(s,x,n) = u_0 + Z^i(s)\,\beta_y(x) + Y^i(s)\;\beta_z(x) - \Omega^i(s)\theta'(x) \quad (1)$$

$$v^i(s,x,n) = -\xi_1^i v_0(x) - \xi_2^i w_0(x) + h^i(s)\theta(x) - \eta^i(s,n)\;\chi(x) \quad (2)$$

$$w^i(s,x,n) = \xi_1^i w_0(x) - \xi_2^i v_0(x) - s\theta(x) + \psi^i(s)\;\chi(x) \quad (3)$$

This expression is a generalization of other previously proposed in the literature (Kim and Yoo 2008; Meftah et al. 2012).

In the above relationships $u_0(x)$, $w_0(x)$ and $v_0(x)$ represent the axial, vertical deflection and lateral displacement in y direction respectively, while $\theta(x)$ denotes the rotation about x. Owing to the contribution of shear deformation, one introduced in the kinematics model the angles $\beta_y(x)$ and $\beta_z(x)$, which measure the rotations about the y and z axes respectively (Fig. 2a–d).

In this formulation (.)' denotes the derivative with respect to the x variable.

The functions $Z^i(s)$, $Y^i(s)$, $\Omega^i(s)$, $h^i(s)$, $\eta^i(s,n)$ and $\overline{\psi^i}(s)$ describe the contour deformations of the beam cross section. They are straightforward to write using box beam theory. They are defined as follows:

$$\begin{aligned}
Z^i(s) &= \left(-\xi_1\frac{h}{2} + \xi_2 s\right)\\
Y^i(s) &= \left(\xi_2\frac{b}{2} + \xi_1 s\right)\\
\Omega^i(s) &= \left(\xi_1^{i^2}\frac{h}{2} - \xi^{i^2}{}_2\frac{b}{2}\right)s\\
h^i(s) &= -\xi_1^i Z^i(s) + \xi_2^i Y^i(s)\\
\eta^i(s,n) &= \xi_1^i Z^i(s) - \xi_2^i Y^i(s) - n\frac{\partial\psi_H^i(s)}{\partial s}\\
\psi^i(s) &= \xi_1^{i^2}\psi_H(s) + \xi_2^{i^2}\psi_V(s)\\
\xi_1 &= \frac{\left[1+(-1)^{i+1}\right]}{2}(2-i),\\
\xi_2 &= \frac{\left[1+(-1)^{i}\right]}{2}(3-i),\\
\psi_v &= \frac{2h}{b+h}\left(\frac{2s^3}{h^2} - \frac{3s}{2}\right)\\
\psi_H &= -\frac{2b}{b+h}\left(\frac{2s^3}{b^2} - \frac{3s}{2}\right)
\end{aligned} \quad (4)$$

In the above formulation, the functions $\psi_H(s)$ and $\psi_V(s)$ are selected to satisfy the in-plane moment equilibrium condition as suggested by Kim and Kim (2002). They may express the in-plane distortion or lozenging deformation denoted by $\chi(x)$ as shown in Fig. 2e.

In the case of thin-walled box section beams, the Green–Lagrange strains tensor which incorporates the large displacements is given by:

$$\varepsilon^{i}_{xx} = u^{i\prime}(s,x,n) + \frac{1}{2}\left(\left(v^{i\prime}(s,x,n)\right)^2 + \left(w^{i\prime}(s,x,n)\right)^2\right) \quad (5\text{-a})$$

$$\varepsilon^{i}_{ss} = -n_i \frac{\partial^2 w^{i}(s,x,n)}{\partial s^2} \quad (5\text{-b})$$

$$\gamma^{i}_{xs} = \frac{\partial u^{i}(s,x,n)}{\partial s} + \frac{\partial v^{i}(s,x,n)}{\partial x} + \frac{\partial v^{i}(s,x,n)}{\partial x}\frac{\partial v^{i}(s,x,n)}{\partial s} + \frac{\partial w^{i}(s,x,n)}{\partial x}\frac{\partial w^{i}(s,x,n)}{\partial s} \quad (5\text{-c})$$

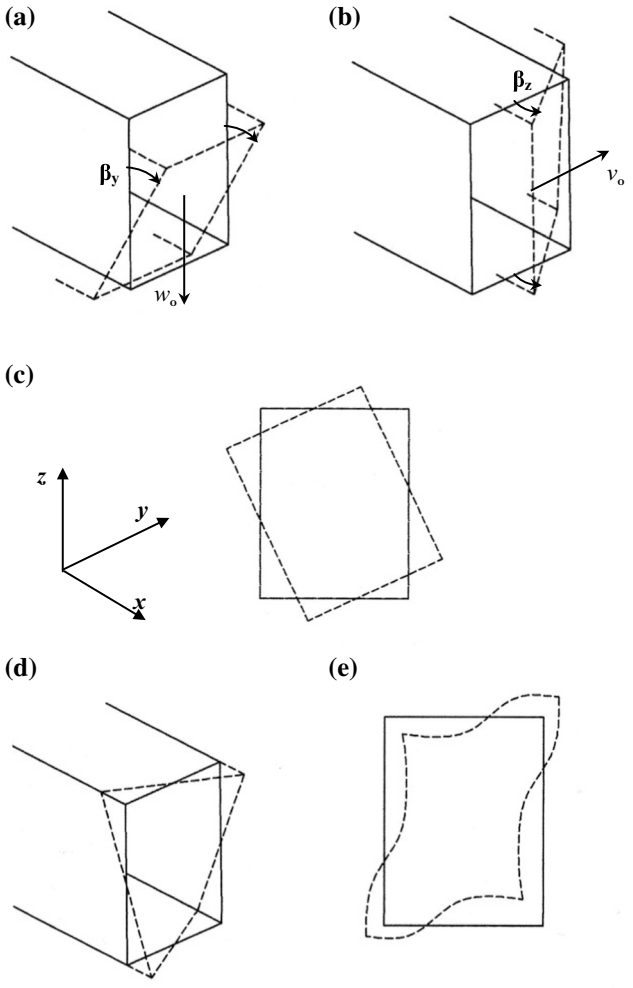

Fig. 2 Deformation shapes of a cross section box beam, **a** bending about y axis, **b** bending about z axis, **c** twisting, **d** warping, e: distortion

After substituting Eqs. (1)–(3) into (5-a), the axial strain can be decomposed into both linear and nonlinear parts as:

$$\varepsilon^{i}_{xx} = \varepsilon^{i}_{l} + \varepsilon^{i}_{nl} \quad (6)$$

while the linear part is given by:

$$\varepsilon^{i}_{l} = u'_0 + Z^{i}(s)\,\beta'_y(x) + Y^{i}(s)\,\beta'_z(x) - \Omega^{i}(s)\,\theta''(x) \quad (7\text{-a})$$

And the nonlinear part, when only the quadratic terms are retained is:

$$\begin{aligned}\varepsilon^{i}{}_{nl} = {} & \frac{1}{2}v'_0(x)^2 + \frac{1}{2}w'_0(x)^2 + \frac{1}{2}\left[h^{i}(s)^2 + s^2\right]\theta'(x)^2 \\ & + \frac{1}{2}\left[\eta^{i}(s,n)^2 + \psi^{i}(s)^2\right]\chi'(x)^2 \\ & - \left[\xi^{i}_1 h^{i}(s) - \xi^{i}_2 s\right]v'_0(x)\theta'(x) \\ & - \left[\xi^{i}_1 \eta^{i}(s,n) + \xi^{i}_2 \psi^{i}(s)\right]v'_0(x)\chi'(x) \\ & - \left[\xi^{i}_1 s + \xi^{i}_2 h^{i}(s)\right]w'_0(x)\theta'(x)\end{aligned} \quad (7\text{-b})$$

The shear strain of the wall unit is:

$$\begin{aligned}\gamma^{i}_{xs} = {} & \xi_2\beta_y(x) + \xi_1\beta_z(x) - \xi^{i}_1 v'_0(x) - \xi^{i}_2 w'_0(x) \\ & + \left[h^{i}(s) - \xi^{i\,2}_1\frac{h}{2} + \xi^{i\,2}_2\frac{b}{2}\right]\theta'(x) + \eta^{i}(s,n)\,\chi'(x)\end{aligned} \quad (8)$$

Once the strain components are defined, the Piola–Kirchhoff stresses tensor for elastic material reads:

$$\begin{Bmatrix}\sigma^{i}_{xx}\\ \tau^{i}_{xs}\end{Bmatrix} = \begin{bmatrix}E_1 & 0\\ 0 & G\end{bmatrix}\begin{Bmatrix}\varepsilon^{i}_{xx}\\ \gamma^{i}_{xs}\end{Bmatrix} \quad (9)$$

where *G and E* are the shear and Young's moduli respectively.

3.2 Variational Formulations

Denoting by U the strain energy of the beam element and by W, the work spent by the external loads, the fundamental equilibrium is obtained by the stationary conditions of total potential, given by

$$\delta(U - W) = 0 \quad (10)$$

where δ denotes the virtual variation.

The variation of the strain energy is:

$$\delta U = \sum_{i=1}^{4}\int_L\int_{F_i}\left(\sigma^{i}_{xx}\delta\varepsilon^{i}_{xx} + \tau^{i}_{xs}\delta\gamma^{i}_{xs}\right)dF_i \quad (11)$$

The above integration is calculated over the cross section area and the beam length L.

By substituting the linear and nonlinear strain–displacement relations given by Eqs. (7-a), (7-b) and (8) and the stress relation Eq (9) into (11), the variation of the strain energy can be formulated as function of the stress resultants acting on the cross section of the box beam, arranged as:

$$\begin{aligned}\delta U = {} & \delta U(N) + \delta U(M_z) + \delta(M_y) + \delta U(B) + \delta U(M_{sv}) \\ & + \delta U(M_R) + \delta U(T_y) + \delta U(T_z) + \delta U(M_\psi) + \delta U(M_{\psi y}) \\ & + \delta U(M_{\psi z}) + \delta U(M_{\psi R}) + \delta U(M_{\psi sv}) \end{aligned} \tag{12}$$

In the above equation, the first terms $\delta U(N)$, $\delta U(M_z)$, $\delta(M_y)$, $\delta U(B)$, $\delta U(M_{sv})$,$\delta U(M_R)$, $\delta U(T_y)$ and $\delta U(T_z)$ represent respectively the contribution of the axial force N, bending moments M_Z and M_y in the z and y directions, warping moment B (bimoment), St-Venant torsion moment M_{sv}, higher order stress resultant, called also Wagner's moment M_R and shear forces T_y and T_z about y and z directions. They are expressed as:

$$\begin{aligned}\delta U(N) = {} & \int_L N\delta u_0'(x)dx + \int_L Nv_0'(x)\delta v_0'(x)dx \\ & + \int_L Nw_0'(x)\delta w_0'(x)dx \\ & + \int_L \frac{2N}{F}\left(A_3 + B_3\right)\theta'(x)\delta\theta'(x)dx \\ & + \int_L \frac{2N}{F}\left(A_{15} + B_{15}\right)\chi'(x)\delta\theta'(x)dx \\ & + \int_L \frac{2N}{F}\left(A_{15} + B_{15}\right)\theta'(x)\delta\chi'(x)dx \\ & + \frac{2N}{F}\left(A_7 + B_7\right)\chi'(x)\delta\chi'(x) \end{aligned} \tag{13-a}$$

$$\begin{aligned}\delta U(M_z) = {} & \int_L M_z\delta\beta_z'(x)dx + \int_L M_y\theta'(x)\,\delta v_0'(x)dx \\ & + \int_L M_y v_0'(x)\delta\theta'(x)\,dx \end{aligned} \tag{13-b}$$

$$\begin{aligned}\delta U(M_y) = {} & \int_L M_y\delta\beta_y'(x)dx - \int_L M_z\theta'(x)\,\delta w_0'(x)dx \\ & - \int_L M_z w_0'(x)\delta\theta'(x)\,dx \end{aligned} \tag{13-c}$$

$$\delta U(B) = \int_L B_\omega\delta\theta''(x)dx \tag{13-d}$$

$$\delta U(M_{sv}) = \int_L M_{sv}\,\delta\theta'(x)dx \tag{13-e}$$

$$\delta U(M_R) = \int_L M_R\theta'(x)\,\delta\theta'(x)dx \tag{13-f}$$

$$\delta U(T_y) = \int_L T_y(\delta v_0' - \delta\beta_z)dx \tag{13-g}$$

$$\delta U(T_z) = \int_L T_z\left(\delta w_0' - \delta\beta_y\right)dx \tag{13-h}$$

Similarly $\delta U(M_\psi)$, $\delta U(M_{\psi z})$, $\delta U(M_{\psi y})$, $\delta U(M_{\psi R})$ and $\delta U(M_{\psi sv})$ are the additional strain energies due to the distortional deformation. They reflect the contribution of the variables ψ_H and ψ_v, given by:

$$\delta U(M_\psi) = \int_L M_\psi\,\chi'(x)\,\delta\chi'(x)dx \tag{14-a}$$

$$\delta U(M_{\psi y}) = \int_L M_{\psi y}\left(\chi'(x)\delta v_0'(x) + v_0'(x)\,\delta\chi'(x)\right)dx \tag{14-b}$$

$$\delta U(M_{\psi z}) = \int_L M_{\psi z}\left(\chi'(x)\delta w_0'(x) + w_0'(x)\delta\chi'(x)\right)dx \tag{14-c}$$

$$\delta U(M_{\psi R}) = \int_L M_{\psi R}\left(\chi'(x)\delta\theta'(x) + \theta'(x)\,\delta\chi'(x)\right)dx \tag{14-d}$$

$$\delta U(M_{sv\psi}) = \int_L M_{sv\psi}\delta\chi'(x)dx \tag{14-e}$$

The global cross section contact actions (N, M_y, M_z, M_{sv}, M_R, T_y, T_z, M_ψ, $M_{\psi y}$, $M_{\psi z}$, $M_{\psi R}$ *and* $M_{\psi sv}$) are described by the usual constitutive equations

$$\begin{aligned}N = E\Bigg[& \left[u_0'(x) + \frac{1}{2}\cdot\left(v_0'^2(x) + w_0'^2(x)\right)\right]F + 2\left(A_{19} + B_{19}\right)\theta'^2(x) \\ & + 2\left(A_{20} + B_{20}\right)\chi'^2(x) + 2\left(A_{15} + B_{15}\right)\theta'(x)\chi'(x)\Bigg] \end{aligned} \tag{15-a}$$

$$\begin{aligned}M_y = E\Bigg[& \left(F_1\frac{h^2}{2} + 2B_1\right)\beta_y'(x) + \left(F_1\frac{h^2}{2} + 2B_1\right)v_0'(x)\theta'(x) \\ & + \left(F_1\frac{h^2}{2} - 2B_2\right)v_0'(x)\chi'(x)\Bigg] \end{aligned} \tag{15-b}$$

$$M_z = E\left[\left(F_2\frac{b^2}{2}+2A_1\right)\beta_z'(x)-\left(F_2\frac{b^2}{2}+2A_1\right)w_0'(x)\theta'(x) +\left(F_2\frac{b^2}{2}+2A_2\right)w_0'(x)\chi'(x)\right] \quad (15\text{-c})$$

$$M_{\psi z} = E\left[\left(F_2\frac{b^2}{2}+2A_2\right)\beta_z'(x)-\left(F_2\frac{b^2}{2}+2A_2\right)w_0'(x)\theta'(x) +\left(F_2\frac{b^2}{2}+2A_{13}+2B_{21}\right)w_0'(x)\chi'(x)\right] \quad (15\text{-g5})$$

$$M_{\psi R} = 2E\left[\begin{array}{l}\left(\left(A_{16}+B_{16}\right)-2\left(A_{15}+B_{15}\right)\dfrac{\left(A_{19}+B_{19}\right)}{A}\right)\theta'^2(x)\\ +\left(\left(A_{17}+B_{17}\right)-2\left(A_{15}+B_{15}\right)\dfrac{\left(A_{20}+B_{20}\right)}{A}\right)\chi'^2(x)\\ +\left(\left(A_{18}+B_{18}\right)-2\left(A_{15}+B_{15}\right)\dfrac{\left(A_{15}+B_{15}\right)}{A}\right)\theta'(x).\chi'(x)\end{array}\right] \quad (15\text{-g6})$$

$$B_\omega = E\left(\frac{h^2}{2}A_1+\frac{b^2}{2}B_1\right)\theta''(x) \quad (15\text{-d})$$

$$M_{sv} = 2Gb\left(bF_2\theta'(x)+B_{23}\chi'(x)\right) \quad (15\text{-e})$$

$$M_R = 2E\left[\begin{array}{l}\left(\left(A_4+B_4\right)-2\left(A_3+B_3\right)\dfrac{\left(A_{19}+B_{19}\right)}{A}\right)\theta'^2(x)\\ +\left(\left(A_5+B_5\right)-2\cdot\left(A_3+B_3\right)\dfrac{\left(A_{20}+B_{20}\right)}{A}\right)\chi'^2(x)\\ +\left(\left(A_6+B_6\right)-2\left(A_3+B_3\right)\dfrac{\left(A_{15}+B_{15}\right)}{A}\right)\theta'(x)\chi'(x)\end{array}\right] \quad (15\text{-f})$$

$$T_y = 2GF_1\left[-\beta_z(x)+v_0'(x)\right] \quad (15\text{-g1})$$

$$T_z = 2GF_2\left[-\beta_y(x)+w_0'(x)\right] \quad (15\text{-g2})$$

$$M_{\psi sv} = 2G\left[bB_{23}\theta'(x)+\left(A_{22}+B_{22}\right)\chi'(x)\right] \quad (15\text{-g7})$$

The expressions of the stiffness coefficients A_i *and* B_j ($i=1,\ldots,23$) may be found in "Appendix" for rectangular box shape section. $F1$ and $F2$ are the cross section areas of the flange and web respectively. While F is the total cross section area of the box beam.

According to Saoula et al. (2016), the variation of the external work for a box beam under combined axial and bending loads with magnitudes q_x and q_z respectively is defined by the relationship:

$$\delta W = \int_L \left(q_x\delta u_0(x)+q_z\delta w_r(s,x)\right)dx \quad (16)$$

The external axial force q_x is applied at the centre line without any eccentricity, while the lateral load q_z is applied along the line (rr') located at the height e_z from the shear centre (Fig. 3).

$$M_\psi = 2E\left[\begin{array}{l}\left(\left(A_8+B_8\right)-2\left(A_7+B_7\right)\dfrac{\left(A_{19}+B_{19}\right)}{A}\right)\theta'^2(x)\\ +\left(\left(A_9+B_9\right)-2\cdot\left(A_7+B_7\right)\dfrac{\left(A_{20}+B_{20}\right)}{A}\right)\chi'^2(x)\\ +\left(\left(A_{11}+B_{11}\right)-2\left(A_7+B_7\right)\dfrac{\left(A_{15}+B_{15}\right)}{A}\right)\theta'(x)\chi'(x)\end{array}\right] \quad (15\text{-g3})$$

$$M_{\psi y} = E\left[\left(F_1\frac{h^2}{2}-2B_2\right)\beta_y'(x)+\left(F_1\frac{h^2}{2}-2B_2\right)v_0'(x)\theta'(x) +\left(F_1\frac{h^2}{2}+2B_{13}+2A_{21}\right)v_0'(x)\chi'(x)\right] \quad (15\text{-g4})$$

In Eq (16), $w_r(s,x)$ is the deflection of (rr') line. This displacement is linked to the shear centre (Eq 3), by considering the quadratic kinematic assumptions as:

$$w_r(s,x) = w_0(x) + e_z\frac{(\theta(x)+\chi(x))^2}{2} \quad (17)$$

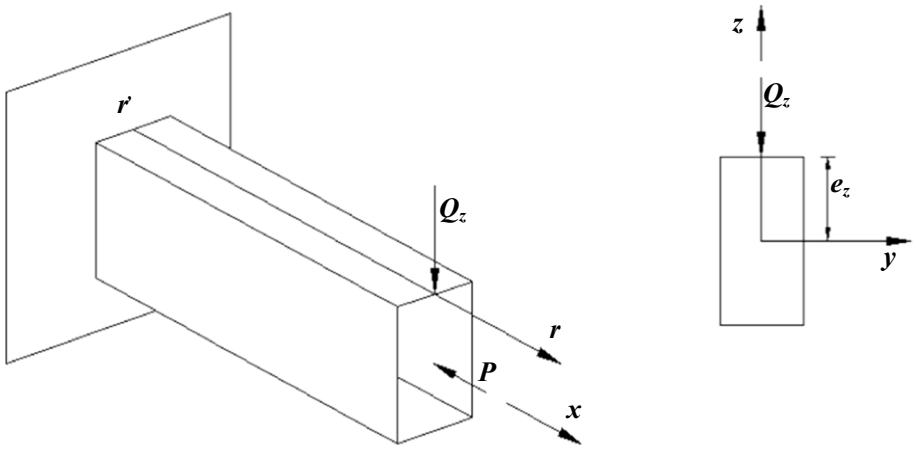

Fig. 3 Cantilever box beam element under axial and lateral concentrated loads at the free end

Using Eq (17) in Eq (16), one gets:

$$\delta W = \int_L \left(q_x \delta u_0(x)\right) dx + \int_L \left(q_z \delta w_0(x)\right) dx + e_z \int_L \left(q_z(\theta(x) + \chi(x))\delta(\theta(x) + \chi(x)\right) dx \tag{18}$$

The eccentricity e_z is called "load height parameter".

According to the equilibrium path expressed by Eq (10) and by considering Eqs. (12)–(14) and (18), the variation of the total potential is written as function of the virtual displacements $\delta u_0(x)$, $\delta v_0(x)$, $w_0(x)$, $\theta(x)$, $\chi(x)$, $\beta_y(x)$ and $\beta_z(x)$, and their derivatives.

Once integrated by parts, for arbitrary variation $\delta u_0(x)$, one gets the equilibrium equation along the axial direction written as:

$$N' = -q_x \tag{19}$$

When axial loads are reduced to a concentric axial force P acting at the beam end, the above relationship becomes:

$$N = -\int_L q_x dx = -P \tag{20}$$

3.3 Numerical Solutions of Lateral Buckling Loads of Cantilever Beam

In order to carry out numerical investigation of LTB resistance of box beams, Ritz method is chosen as a solution procedure. According to Ritz's method, the solution of eigenvalue equation for continuous structural system can be expressed in term of linear combination of selected shape functions.

When applying the Ritz's method, the shape functions are chosen to satisfy only the boundary conditions and not necessarily the equilibrium ones.

In the case of cantilever box beams, the following polynomial functions forms are used

$$\left\{ v_0(x)\ w_0(x)\ \theta(x) \quad \chi(x) \right\} = \sum_{i=1}^{N} \left\{ v_i\ w_i\ \theta_i \quad \chi_i \right\} \left(\frac{x}{L}\right)^{i+1} \tag{21-a}$$

$$\left\{ \beta_y(x)\ \beta_z(x) \right\} = \sum_{i=1}^{N} \left\{ \beta_{yi}\ \beta_{zi} \right\} \left(\frac{x}{L}\right)^{i} \tag{21-b}$$

And their virtual variation forms are:

$$\left\{ \delta v_0(x)\ \delta w_0(x)\ \delta\theta(x) \quad \delta\chi(x) \right\} = \sum_{i=1}^{n} \left\{ \delta v_i\ \delta w_i\ \delta\theta_i \quad \delta\chi_i \right\} \left(\frac{x}{L}\right)^{i+1} \tag{22-a}$$

$$\left\{ \delta\beta_y(x)\ \delta\beta_z(x) \right\} = \sum_{i=1}^{n} \left\{ \delta\beta_{yi}\ \delta\beta_{zi} \right\} \left(\frac{x}{L}\right)^{i} \tag{22-b}$$

Where v_i, w_i, θ_i, χ_i, β_{yi} and β_{zi} are the associated displacements and rotations amplitudes.

After substituting Eqs. (13) and (14) into Eq (12) and making use of Eqs. (15), (18) and (21), 5 N coupled equilibrium equations are derived from Eq (10), by using the gradient operator as follow:

$$\{f\} = grad(\delta(U - W), \{\delta d\}) = \{0\} \tag{23}$$

where $\{f\}$ is a general residual that governs the non linear problem and the vector δd is the variation of Ritz coefficients given by:

$$\delta d = \left\{ \{\delta v_i\}, \{\delta w_i\}, \{\delta\theta_i\}, \{\delta\chi_i\}, \{\delta\beta_{yi}\}, \{\delta\beta_{zi}\} \right\}^T \tag{24}$$

It should be noted that, the equilibrium equations are nonlinear and highly coupled.

At this stage, one gets the tangent matrix K_t which is defined as the Jacobian matrix of the general residual $\{f\}$ given in Eq (23), with respect to the Ritz coefficients Eq (21). The stability analysis of box beams is analyzed by taking into account the initial deflection in the prebuckling state (fundamental

state). It is reasonable to assume that the fundamental state may be obtained by requiring the condition of singularity of the tangent stiffness matrix ($det\ K_t = 0$).

4 Comparison Study

The analytical model presented in this work was implemented using Matlab code (MATLAB 2006). To verify the accuracy of the present analytical model, the critical buckling loads Q_{cr} of cantilever box columns under compressive loads obtained by the present approach were compared with those from the 3D FEM commercial package ABAQUS (2003). In the 3D FE simulation employed in this investigation, each box column is modelled with appropriate sizes meshes by thin shell elementsS8R, including five integration points through the thickness (Fig. 4). This element accounts for transverse shear deformations and can automatically generate the mesh. This permits also to make easy the introduction of the applied lateral load, either at the top or bottom flanges or at the shear center of the beam section.

It is worth noting that, the concentrated load is applied through the mid-line of the S8R elements and was distributed along the cross section width to reflect the elastic lateral torsional nuckling behaviour of the members in real FEM simulation.

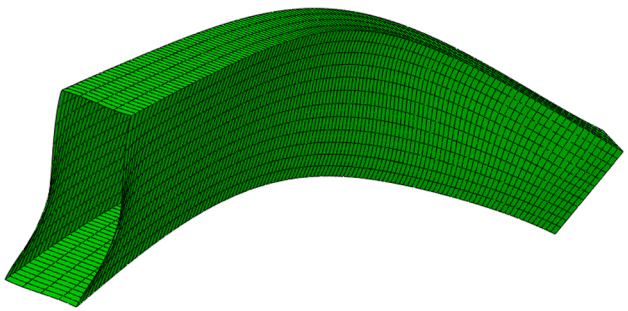

Fig. 4 View of uniform shell mesh adopted for the cantilever box beam with distortional deformation along the beam contour

In the attempt to satisfy rigid section assumption for the cantilever beam near the clamped region and therefore, to prevent local deformations involved by shell element modeling, stiffeners elements are used for this goal. The stiffeners are modeled by using beam element B32 placed along the sectional contour using stringer Abaqus option. The stiffener section is chosen to satisfy a rigid profile condition without any additional stiffnesses.

In order to find the critical loads, for the all studied specimen box columns, the Lanczos eigensolver of ABAQUS (2003) was used to conduct elastic buckling analysis.

However, it can be useful to verify the results of the present model with those given by the classical method when the distortional deformation is neglected. The relative errors were calculated according to:

$$\Delta_1 = \frac{\left|Q_{cr}(Present) - Q_{cr}(Abaqus)\right|}{Q_{cr}(Abaqus)} \tag{25-a}$$

$$\Delta_2 = \frac{\left|Q_{cr}(Classic) - Q_{cr}(Abaqus)\right|}{Q_{cr}(Abaqus)} \tag{25-b}$$

4.1 Example 1

In this example, the lateral buckling stability of rectangular cantilever box columns under top flange uniformly distributed loads and compressive concentrated forces applied at the free edgesare investigated. Two cross sections with wall thickness of 3 and 4 mm respectively are considered for the analysis. The columns slenderness has been varied from 1.5 to 2.5 m. In addition, we use the standard rectangular box beam dimensions $h = 100$ mm and $b = 50$ mm. In this example, the modulus of elasticity of the material and Poisson's ratio are assumed to 210GPa and 0.3 respectively.

Table 1 gives lateral buckling loads obtained by increasing the number N of the power series terms, in the case of axially unloaded cantilever beams. One remarks, that the

Table 1 Cantilever box beam load on upper flange (e_z = 50 mm), Buckling loads comparisons without applied axial forces ($h = 100$ mm, b = 50 mm)

L (m)	T (mm)	Q_{cr} (Present) with $N = 2$ (KN)	Q_{cr} (Present) with $N = 3$ (KN)	Q_{cr} (Present) with $N = 4$ (KN)	Q_{cr} (Present) with $N = 5$ (KN)	Q_{cr} (Present) with $N = 6$ (KN)	Q_{cr} (FEM) (KN)
1.5	3	229.51	226.36	223.80	223.45	223.45	199.96
	4	306.127	329.21	325.13	324.66	324.66	306.45
2	3	98.17	97.13	96.13	96.03	96.03	96.67
	4	130.94	141.47	139.86	139.71	139.71	143.94
2.5	3	50.665	50.24	54.28	54.23	54.23	49.90
	4	67.58	73.20	72.40	72.33	72.33	72.64

buckling loads converge when the number N is increased ($N \geq 3$).

As part of the validation, the buckling loads of the box columns subjected to compressive loads are calculated and listed in Table 2, and well compared to FEM results. These outcomes provide that acceptable convergence is obtained for $N \geq 3$. Furthermore, an important error $\Delta_1 = 12\%$ is observed in the case of short box beam with $L = 1.5$ m and $t = 3$ mm and without compressive load.

4.2 Example 2

This example consists of a cantilever steel box beam loaded by concentrated loads at the free edge as shown in Fig. 5. The cross section dimensions are $h = 600$ mm, $b = 200$ mm. In the present study, both the cross section thickness t and length L have been varied. For this example the modulus of elasticity and Poisson's ratio are assumed to $E = 210$GPa and $\nu = 0.3$.

Tables 3, 4 and 5 shows the lateral buckling loads given by different methods. These loads are evaluated with different load height positions ($e_z = 300$, 0.0 and -300 mm), these ones correspond to top flange; shear centre and bottom flange locations respectively. These outcomes lead to the following remarks:

1. There is excellent agreement between the elastic buckling loads provided by the FEM simulation and the present study with a relative error $\mathbf{\Delta_1 \leq 7\%}$.
2. Important error Δ_2 more than 50%, is observed especially in the case of short beam (L=6 m). It is evident that, classical solution such as adopted in EC3is not

Table 2 Cantilever box beam load on upper flange ($e_z = 50$ mm), Buckling loads comparisons with applied compressive force P($h = 100$ mm, $b = 50$ mm)

L (m)	T (mm)	P (KN)	Q_{cr} (Present) with $N=2$ (KN)	Q_{cr} (Present) with $N=3$ (KN)	Q_{cr} (Present) with $N=4$ (KN)	Q_{cr} (Present) with $N=6$ (KN)	Q_{cr} (Present) with $N=6$ (KN)	Q_{cr} (FEM) (KN)
1.5	3	80	70.46	74.68	74.63	74.63	74.63	74.65
	4		147.47	157.68	157.45	157.45	157.45	153.49
2	3	40	37.77	40.25	40.22	40.22	40.22	39.62
	4		70.24	75.34	75.21	75.21	75.21	77.6
2.5	3	30	13.92	14.70	14.69	14.69	14.69	15.84
	4		30.90	33.07	33.03	33.03	33.03	36.54

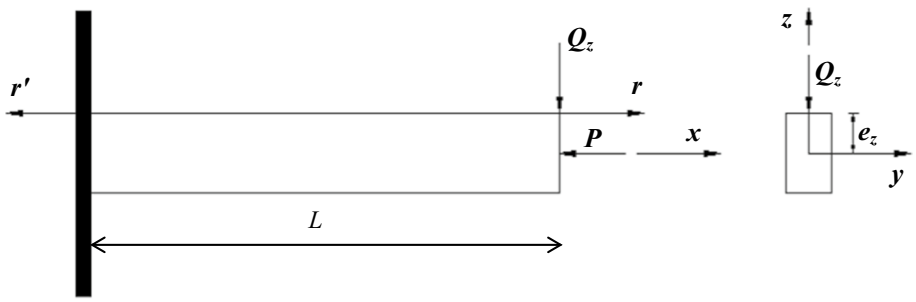

Fig. 5 Cantilever box beam element considered in the study

Table 3 Cantilever box beam load on upper flange (e_z=300 mm) under compressive force, Buckling loads comparisons and relative errors

L (m)	T (mm)	P (KN)	Q_{cr} (Present) with $N=3$ (KN)	Q_{cr} (Classic) (KN)	Q_{cr} (FEM) (KN)	Δ_1% (Present/ FEM)	Δ_2% (Classic/ FEM)
6	20	2000 KN	3141.12	5730.34	3164.0	0.72	81.11
	25		4750.21	7864.22	4728.6	0.46	66.31
	20	1000 KN	2068.50	3473.96	2065.0	0.17	68.23
8	25		2841.77	4695.97	2976.0	4.5	57.80
10	20	500 KN	1480.26	2452.35	1535.9	3.62	59.70
	25		1975.20	3236.52	2124.5	7.02	52.43

Table 4 Cantilever box beam load on shear centre (e_z=0.00 mm) under compressive force, Buckling loads comparisons and relative errors

L (m)	T (mm)	P (KN)	Q_{cr} (Present) with $N=3$ (KN)	Q_{cr} (Classic) (KN)	Q_{cr} (FEM) (KN)	Δ_1% (Present/FEM)	Δ_2% (Classic/FEM)
6	20	2000 KN	3252.84	6019.02	3225.4	0.85	86.61
	25		4969.94	8311.48	4875.4	1.94	70.50
	20	1000 KN	2135.92	3612.23	2105.5	1.44	71.56
8	25		2944.91	4902.09	3051.0	3.48	60.67
10	20	500 KN	1523.41	2538.06	1566.4	2.74	62.03
	25		2037.18	3357.43	2175.0	6.33	54.36

Table 5 Cantilever box beam load on bottom flange (e_z=− 300 mm) under compressive force, Buckling loads comparisons and relative errors

L (m)	t (mm)	P (KN)	Q_{cr} (Present) with $N=3$ (KN)	Q_{cr} (Classic) (KN)	Q_{cr} (FEM) (KN)	Δ_1% (Present/FEM)	Δ_2% (Classic/FEM)
6	20	2000 KN	3362.75	6273.81	3244.9	3.63	93.34
	25		5188.03	8702.09	4908.1	5.70	77.30
	20	1000 KN	2202.95	3737.501	2123.3	3.75	76.02
8	25		3047.52	5087.55	3088.4	1.32	64.73
10	20	500 KN	1566.40	2616.76	1582.2	1	65.39
	25		2098.95	6273.81	2203.5	4.74	57.38

appropriate. Therefore, the EC3 solution must be then questioned in the case of box beam elements.

3. It can be remarked from this example that no significant effect has been reported for the load height location e_z on the critical loads.

5 Parametric Study Based on the EC3

5.1 Design Approach Accordance with EN 15512 (EC3) (Kim and Kim 1999)

According to the EN 15512 (Eurocode 3) (Benyamina et al. 2013) rack provisions, that is guidance for the principle for racks monotonic design but it represents, at the same time, the reference for verification of members subjected to seismic loading. The resistance of laterally unrestrained column elements under axial load P and bending moment about the principal cross section axis M_{Ed} should be verified according to the following condition

$$\frac{P}{\chi_{\min} A f_y} + \frac{K_{LT} M_{Ed}}{\chi_{LT} W_{pl} f_y} \leq 1 \tag{26}$$

where χ is the reduction factor due to the LTB, W_{pl} is the plastic section modulus and f_y is the material yielding strength.

The evaluation of the relative slenderness $\bar{\lambda}$ for axial load is at first required, which is defined as:

$$\bar{\lambda} = \sqrt{\frac{N_{RD}}{P_{cr}}} \tag{27}$$

where N_{RD} is the characteristic resistance for compression:

$$N_{RD} = A f_y \tag{28}$$

The term $\chi_{\min}$ is the reduction factor due to flexural buckling, it depends strictly on the maximum value of the relative slenderness $\bar{\lambda}$, being defined as:

$$\chi_{\min} = \frac{1}{\phi + \sqrt{\phi^2 - \bar{\lambda}^2}} \leq 1 \tag{29}$$

and ϕ is given by:

$$\phi = 0.5\left[1 + 0.34(\bar{\lambda} - 0.2) + \bar{\lambda}^2\right] \tag{30}$$

As to the contribution due to the bending moment about the principal major axis, the LTB reduction factor χ_{LT} can be determined via expression (27) by substituting the relative slenderness for axial load $\bar{\lambda}$ to that of LTB $\bar{\lambda}_{LT}$ defined as:

$$\bar{\lambda}_{LT} = \sqrt{\frac{M_{pl,RD}}{M_{cr}}} \tag{31}$$

M_{cr} is the elastic critical moment for LTB. This one (M_{cr}) may be carrying out by the present model, ABAQUS and the classical model when the distortional deformation is disregarded.

$M_{pl,RD}$ is the plastic resistance moment given by:

$$M_{pl,RD} = W_{pl} f_y \tag{32}$$

The term K_{LT} is defined as:

$$K_{LT} = 1 - \frac{\mu_{LT} P}{\chi_z A f_y} \leq 1 \tag{33}$$

with μ_{LT} is given by:

$$\mu_{LT} = 0.15\left(\bar{\lambda}_z \beta_{M,LT} - 1\right) \leq 0.9 \tag{34}$$

where $\bar{\lambda}_z$ is the slenderness ratio for flexural buckling and $\beta_{M,LT}$ is an equivalent uniform moment factor for lateral–torsional buckling. This one is taken equal 1.8 for cantilever beams.

According to Eq (26), to check the moment carrying capacity of laterally unrestrained box beam under axial load and bending moment, the following expression has to be fulfilled

$$\frac{M_{Ed}}{M_{pl,Rd}} \leq \frac{M_{SD}}{M_{pl,Rd}} = \frac{\chi_{LT}}{K_{LT}}\left(1 - \frac{P}{\chi_{\min} A f_y}\right) \tag{35}$$

The purpose of this study is to illustrate the impact of the current elastic critical moment (M_{cr}) on the bending moment carrying capacity ratio $M_{SD}/M_{pl,RD}$. One reminds, for comparison, that the critical moment is determined by the proposed method, ABAQUS and the classical method.

In this study the cross section dimensions of the example 3 with $t = 20$ mm is retained in the parametric investigation.

5.2 Compressive Load Effect on the Moment Carrying Capacity Ratio $M_{SD}/M_{pl,RD}$

The variations of the moment carrying capacity ratio $M_{SD}/M_{pl,RD}$ computed from the different approaches of M_{cr} (i.e. proposed model, ABAQUS and classical method) in function of axial load ratio P/P_{cr} are drawn in Fig. 6a–c. The steel yielding strength f_y is equal to 345 MPa. As expected, the ratio $M_{SD}/M_{pl,RD}$ is larger for lower compressive loads. These interaction curves state, that M_{SD} resulting from the proposed model agree very well with the FEM solution, while the classical method tends to overestimate tremendously the real values of M_{SD}.

In the case of cantilever beams under compressive loads, the interaction curves decrease nonlinearly from the pure design moment $M_{SD}(0)$ when P is null to the vanished value when P reaches its critical value P_{cr}.

In the case of a short cantilever box beam with $L = 6$ m (Fig. 6a), the relative error related to the proposed model is varied from 0.5% for $P/P_{cr} = 0$ to 00% for $P/P_{cr} = 0.8$, whereas the error provided by classical method varies continuously from 10% for $P/P_{cr} = 0$ to 29% for $P/P_{cr} = 0.8$. For the box beam with $L = 8$ m (Fig. 6b), the relative error

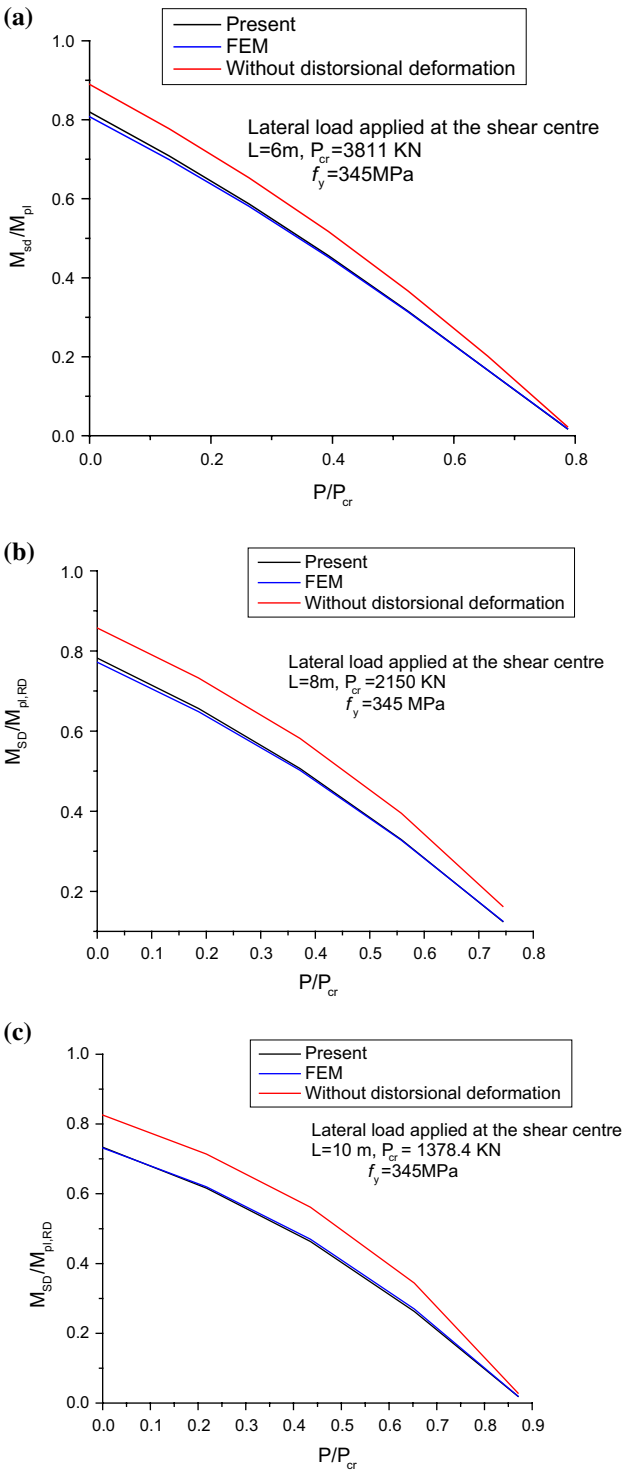

Fig. 6 Interaction of maximal design moment with axial load ration for cantilever box beam under free edge load located at centroid. **a** Box beam with $L = 6$ m, **b** Box beam with $L = 8$ m and **c** Box beam with $L = 10$ m

corresponding to the proposed model is stable without major change (between 0.7% to 2%). Whereas, according to the classical method, the error changes dramatically from 11 to 29%.

In the slender cantilever box beam with $L=10$ m, the results depicted in Fig. 6c show, that the relative error given by the proposed model vary from 1.3 to 9%. This one becomes very pronounced when the classical method is employed. The relevant relative error is between 13 to 43%.

From this study, it was clearly demonstrated that the critical LTB moment M_{cr} given by the proposed model leads to a satisfactory approximation of the moment carrying capacity M_{SD}.

Investigation into the effect of yielding strength f_y on the moment carrying capacity ratio $M_{SD}/M_{pl,RD}$ is carried out for a cantilever beam with $L = 10$ m. This beam is tested by varying the applied axial load ratio P/P_{cr} from 0 to 0.9. Three steel nuances are considered in this study. The two first ones correspond to the structural grade steel S275 and S355 with $f_y = 265$ and 345 MPa respectively, whereas, the last onecorresponds to the high yield steel S700MC with $f_y = 700$ MPa.

Figure 7a–c show the differences that refer to the FEM results. The difference $\delta_1$is related to the present model and δ_2 is of the classical method.

These outcomes reveal that, the present method achieves a very good agreement compared to FEM. The classical theory tends to overestimate the real resistance of the structure. Figure 7a represents the evolution of the differences δ_1 and $\delta_2$as function of the ratio P/P_{cr} for the structural steel S275. Again, it is confirmed that the proposed method provides in general similar results compared to FEM. In this way δ_1 is lower than 8%. One observes from Fig. 7a that, omitting the distortional deformation can lead to rigid beam behavior. Thus the differences in δ_2 are important.

The differences δ_1 and δ_2 for the structural steel S355 are illustrated in Fig. 7b. These curves demonstratethe ability of the present model to predict correctly the resistance of the cantilever box beams under axial loads. One gets a differenceδ_1 smaller than 9%, while the classical method leads to δ_2 reaching the value of 43%.

In order to appreciate better the effect of the yielding strength on the moment carrying capacity ratio $M_{SD}/M_{pl,RD}$, cantilever box beam structures made of high yield steel S700MC are studied. The observation of the results reported in Fig. 7c prompts the following comments:

1. The proposed model furnishes a satisfactory approximation to prevent the structural integrity, under combined axial and lateral loads. The difference $\delta_1$varies from 2 to 11% for $P/P_{cr}=0.9$.
2. The classical method is inappropriate for the structural design of box beam elements. The results involve a difference $\delta_2$larger than 27% and close to57% for $P/P_{cr}=0.9$.

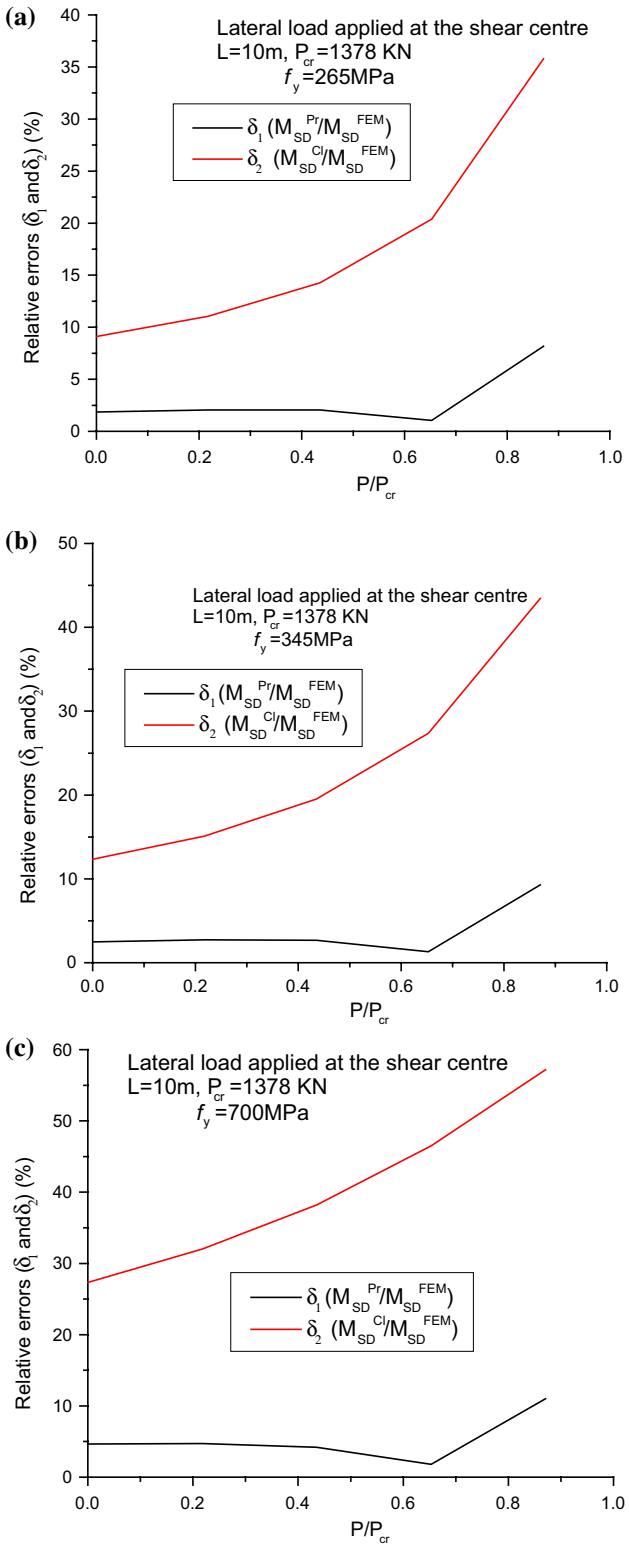

Fig. 7 Effect of the applied axial load ratio on the differences δ_1 and δ_2 for cantilever box beam. **a** Box beam made with steel S275, **b** Box beam made with steel S355, **c** Box beam made with steel S700MC

6 Conclusion

In this work the LTB behavior of steel box beams was investigated. An improved kinematic model that takes account both distortional and shear deformations of the beam cross section was presented. Based on the polynomial shape functions, Ritz's method was applied to provide the tangential matrix of cantilever box beams. This permits the determination of the critical load from the fundamental state.

It has been confirmed that the present model is close to FEM. The buckling loads are similar. However, the classical method leads to significant discrepancies in comparison with FEM. The critical loads are very high than FEM.

According to EC3 guidelines, a parametric study was performed to investigate the influences of several parameters related to M_{cr} evaluation, on the moment carrying capacity of cantilever box beam, namely, the compressive load ratio *P/Pcr*, beam length and steel grade.

The obtained results reveal that the proposed method is more rational than the classical one, with an error averaging 4%. Comparisons also show that, using classical method yields unreliable moment carrying capacity, especially for the box beams made with high yield steel such as S700MC. The relevant error reached 57%. Thus, this method must be considered cautiously.

It was found, from the outcomes of this conceptual study, that the proposed method is simple and accurate enough to be used both at preliminary design stage and at final verification of the box beam elements.

Appendix: Box Cross Section Constants

$$\left(We\ consider:\ t_f = t_w = t\right)$$

$$A_1 = \frac{1}{12}b^3t$$

$$A_2 = \frac{1}{5}\frac{b^4t}{b+h}$$

$$A_3 = \frac{1}{4}h^2bt + \frac{1}{12}b^3t$$

$$A_4 = \frac{1}{160}b^5t + \frac{1}{48}h^2b^3t + \frac{1}{32}h^4bt$$

$$A_5 = \frac{9}{144}\left(\frac{1}{2}\frac{b^2}{(b+h)^2} - \frac{h^2}{(b+h)^2}\right)b^3t^3 + \frac{9}{480}\left(\frac{h^2}{b^2(b+h)^2} - \frac{2}{(b+h)^2}\right)b^5t^3 + \frac{9}{672}\frac{b^5t^3}{(b+h)^2} + \frac{9}{96}\frac{b^3h^2t^3}{(b+h)^2} + \frac{1}{288}\frac{b^7t}{(b+h)^2} + \frac{1}{224}\left(\frac{h^2}{b^2(b+h)^2} - \frac{6}{(b+h)^2}\right)b^7t + \frac{1}{96}\left(\frac{9b^2h^2}{(b+h)^2} + h^2\right)b^3t + \frac{3}{80}\left(\frac{3}{2}\frac{b^2}{(b+h)^2} - \frac{h^2}{(b+h)^2}\right)b^5t + \frac{1}{32}h^4bt$$

$$A_6 = \frac{1}{112}\frac{b^6t}{b+h} + \frac{1}{80}\left(\frac{h^2}{b(b+h)} - \frac{3b}{b+h}\right)b^5t - \frac{1}{48}\left(h^2 - \frac{3h^2b}{b+h}\right)b^3t - \frac{1}{16}h^4bt$$

$$A_7 = \frac{2}{5}\frac{b^3t^3}{(b+h)^2} + \frac{17}{35}\frac{b^5t}{(b+h)^2} + \frac{1}{4}h^2bt$$

$$A_8 = \frac{9}{144}\left(\frac{b^2}{2(b+h)^2} - \frac{h^2}{(b+h)^2}\right)b^3t^3 + \frac{9}{480}\left(\frac{h^2}{b^2(b+h)^2} - \frac{2}{(b+h)^2}\right)b^5t^3 + \frac{9}{672}\frac{b^5t^3}{(b+h)^2} + \frac{9}{96}\frac{b^3h^2t^3}{(b+h)^2} + \frac{1}{288}\frac{b^7t}{(b+h)^2} + \frac{1}{224}\left(\frac{h^2}{b^2(b+h)^2} - \frac{6}{(b+h)^2}\right)b^7t + \frac{1}{12}\left(\frac{9}{8}\frac{b^2h^2}{(b+h)^2} + \frac{h^2}{8}\right)b^3t + \frac{3}{80}\left(\frac{3}{2}\frac{b^2}{(b+h)^2} - \frac{h^2}{(b+h)^2}\right)b^5t + \frac{1}{32}h^4bt$$

$$A_9 = \frac{36}{175}\frac{b^5t^5}{(b+h)^4} + \frac{1625}{3696}\frac{b^7t^3}{(b+h)^4} + \frac{27}{144}\left(\frac{3b^4}{(b+h)^4} - \frac{2h^2}{(b+h)^2}\right)b^3t^3 + \frac{27}{48}\frac{b^3h^2t^3}{(b+h)^2} + \frac{27}{240}\left(\frac{h^2}{b^2(b+h)^2} - \frac{8b^2}{(b+h)^4}\right)b^5t^3 + \frac{713}{4576}\frac{b^9t}{(b+h)^4} + \frac{3}{16}\frac{b^5h^2t}{(b+h)^2} + \frac{1}{32}h^4bt + \frac{1}{112}\left(\frac{h^2}{b^2(b+h)^2} - \frac{54b^2}{(b+h)^4}\right)b^7t + \frac{3}{80}\left(\frac{27}{2}\frac{b^4}{(b+h)^4} - \frac{2h^2}{(b+h)^2}\right)b^5t$$

$$A_{10} = -\frac{1}{24}b^3ht - \frac{1}{8}h^3bt$$

$$A_{11} = -\frac{19}{168}\frac{b^6t^3}{(b+h)^3} + \frac{3}{80}\left(\frac{7b}{(b+h)^3} + \frac{3h^2}{b^2(b+h)^2}\right)b^5t^3 - \frac{27}{144}\left(\frac{b^3}{(b+h)^3} + \frac{2h^2}{(b+h)^2}\right)b^3t^3 + \frac{27}{48}\frac{b^3h^2t^3}{(b+h)^2} - \frac{5}{88}\frac{b^8t}{(b+h)^3} + \frac{1}{16}h^4bt + \frac{1}{112}\left(\frac{h^2}{b^2(b+h)^2} + \frac{27b}{(b+h)^3}\right)b^7t + \frac{1}{80}\left(\frac{h^2}{b(b+h)} - \frac{27b^3}{(b+h)^3} - \frac{6h^2}{(b+h)^2}\right)b^5t + \frac{3}{48}\left(\frac{3b^2h^2}{(b+h)^2} - \frac{h^2b}{b+h}\right)b^3t$$

$$A_{12} = \frac{3}{5}\frac{b^3ht^3}{(b+h)^2} + \frac{17}{70}\frac{b^5ht}{(b+h)^2} + \frac{1}{8}h^3bt$$

$$A_{13} = \frac{17}{35}\frac{b^5t}{(b+h)^2}$$

$$A_{14} = \frac{1}{5}\frac{b^3ht^3}{(b+h)^2} - \frac{1}{10}\frac{b^4ht}{b+h} + \frac{1}{8}h^3bt$$

$$A_{15} = -\frac{1}{5}\frac{b^4t}{b+h} + \frac{1}{4}h^2bt$$

$$A_{19} = \frac{1}{8}h^2bt + \frac{1}{24}b^3t$$

$$A_{20} = \frac{1}{5}\frac{b^3t^3}{(b+h)^2} + \frac{17}{70}\frac{b^5t}{(b+h)^2} + \frac{1}{8}h^2bt$$

$$A_{21} = \frac{2}{5}\frac{b^3t^3}{(b+h)^2}$$

$$A_{22} = \frac{2}{5}\frac{b^3t^3}{(b+h)^2} + \frac{1}{4}h^2bt$$

$$A_{23} = \frac{1}{2}hbt$$

$$A_{16} = \frac{1}{224}\frac{b^6t}{b+h} + \frac{1}{160}\left(\frac{h^2}{b(b+h)} - \frac{3b}{b+h}\right)b^5t + \frac{1}{96}\left(h^2 - \frac{3h^2b}{(b+h)^2}\right)b^3t + \frac{1}{32}h^4bt$$

$$A_{17} = -\frac{19}{336}\frac{b^6t^3}{(b+h)^3} + \frac{9}{480}\left(\frac{7b}{(b+h)^3} + \frac{3h^2}{b^2(b+h)^2}\right)b^5t^3 - \frac{27}{144}\left(\frac{b^3}{2(b+h)^3} + \frac{h^2}{(b+h)^2}\right)b^3t^3 + \frac{27}{96}\frac{b^3h^2t^3}{(b+h)^2} - \frac{5}{176}\frac{b^8t}{(b+h)^3} + \frac{1}{32}h^4bt + \frac{1}{224}\left(\frac{h^2}{b^2(b+h)^2} + \frac{27b}{(b+h)^3}\right)b^7t + \frac{1}{80}\left(\frac{h^2}{2b(b+h)} - \frac{27b^3}{2(b+h)^3} - \frac{3h^2}{(b+h)^2}\right)b^5t + \frac{3}{96}\left(\frac{3b^2h^2}{(b+h)^2} - \frac{h^2b}{b+h}\right)b^3t$$

$$A_{18} = \frac{1}{10}\frac{b^3h^2t^3}{(b+h)^2} - \frac{47}{1008}\frac{b^7t}{(b+h)^2} - \frac{1}{8}\frac{b^4h^2t}{b+h} + \frac{1}{80}\left(\frac{2h^2}{b(b+h)} + \frac{9b^2}{(b+h)^2}\right)b^5t + \frac{1}{16}h^4bt$$

The B_j (j = 1,…,22) coefficients are computed in the same fashion as A_j by replacing reciprocally b by h. As an example according to the constant A_1 defined previously, the similar constant B_1 is:

$$B_1 = \frac{1}{12}h^3 t$$

References

ABAQUS. (2003). *ABAQUS standard user's manual, version 6.4*. Pawtucket: Hibbit, Karlsson and Sorensen Inc.

AISC LRDF, & American Institute of Steel Construction (AISC). (1994). *Load and resistance factor design*. Chicago: AISC.

Asgarian, B., Soltani, M., & Mohri, F. (2013). Lateral-torsional buckling of tapered thin-walled beams with arbitrary cross-sections. *Thin-Walled Structures, 62,* 96–108.

Balch, C. D. (1986). End effects in thin-walled box beam and tubular frame joints. *Ph.D. Dissertation*, Stanford University, Stanford, CA.

Balch, C. D., & Steele, C. R. (1987). Asymptotic solutions for warping and distortion of thin-walled box beams. *Journal of Applied Mechanics, 54,* 165–173.

Benyamina, A. B., Meftah, S. A., Mohri, F., & Daya, E. M. (2013). Analytical solutions attempt for lateral torsional buckling of doubly symmetric web-tapered I-beams. *Engineering Structures, 56,* 1207–1219.

Boitzov, G. V. (1972). Analiz Poperechnoi Prochnosti Krupnotonnaznih Tankerov [Analysis of the transverse strength of large tankers]. *Sudostroenie, 9,* 17–24.

Boswell, L. F., & Li, Q. (1995). Consideration of the relationships between torsion, distortion and warping of thin-walled beams. *Thin-Walled Structures, 21,* 147–161.

Boswell, L. F., & Zhang, S. H. (1984). The effect of distortion in thin-walled beams. *International Journal of Solids and Structures, 20*(9/10), 845–862.

Braham, M., Rondal, J., & Massonet, C. (1980). Large size buckling tests on steel columns with thin-walled rectangular hollow sections. Comparison with design methods. In J. Rhodes & A. C. Walker (Eds.), *Thin-walled structures*. London: Granada Publishers.

Bull, J. W. (1988). *Finite element analysis of thin-walled structures*. London–New York: Elsevier.

Choi, S., & Kim, Y. Y. (2016a). Analysis of two box beams-joint systems under in-plane bending and axial loads by one-dimensional higher-order beam theory. *International Journal of Solids and Structures, 90,* 69–94.

Choi, S., & Kim, Y. Y. (2016b). Exact matching at a joint of multiply-connected box beams under out-of-plane bending and torsion. *Engineering Structures, 124,* 96–112.

Eurocode 3. (1992). Design of steel structures, Part 1.1: General rules of buildings European committee for Standardisation. *Draft Document ENV 1993-1-1*, Brussels.

Gang, W. J., Soo, M. C., & Yoo, Y. K. (2013). Analysis of three thin walled box beam connected at a joint under out of plane bending loads. *Journal of Engineering Mechanics, 139,* 1350–1361.

Graves Smith, T. R. (1967). The ultimate strength of locally buckled columns of arbitrary length. In *Symposium on thin-walled steel constructions*, University College, Swansea.

Graves Smith, T. R. (1971). The effect of initial imperfections on the strength of thin-walled box columns. *International Journal of Mechanical Sciences, 13,* 911–925.

Gupta, N. K., Ray, P., Gupta, S. K., & Khullar, A. (2000). Lateral collapse of empty and filled square aluminium tubes between two platens. In N. K. Gupta (Ed.), *Plasticity and impact mechanics (Proc IMPLAST'96, Delhi)*. Rolla: University of Missouri-Rolla.

Hsu, Y. T., Fu, C. C., & Scheling, D. R. (1995). EBEF method for distortional analysis of steel box girder bridges. *Journal of Structural Engineering, 121*(3), 557–566.

Hughes, O. W. (1983). *Ship structural design*. New York: Wiley.

Jombock, J. R, & Clark, J. W. (1961). Postbuckling behaviour of flat plates. In *Proceedings of ASCE,* 87(ST5).

Kim, J. H., & Kim, Y. Y. (1999). Thin walled closed box beam element for static and dynamic analysis. *International Journal for Numerical Methods in Engineering, 45,* 473–490.

Kim, J. H., & Kim, Y. Y. (2000). One-dimensional analysis of thin walled closed beams having general cross-sections. *International Journal for Numerical Methods in Engineering, 49,* 653–668.

Kim, Y. Y., & Kim, Y. (2002). A one-dimensional theory of thin-walled curved rectangular box-beam under torsion and out-of-plane bending. *International Journal for Numerical Methods in Engineering, 53,* 1675–1693.

Kim, K., & Yoo, C. H. (2008). Ultimate strengths of steel rectangular box beams subjected to combined action of bending and torsion. *Engineering Structures, 30,* 1677–1687.

MATLAB 7.1. (2006). Natick: The MathWorks Inc.

Meftah, S. A., Daya, E. M., & Tounsi, A. (2012). Finite element modelling of sandwichbox column with viscoelastic layer for passive vibrations control under seismic loading. *Thin-Walled Structures, 50,* 174–185.

Mohri, F., Meftah, S. A., & Damil, N. (2015). A large torsion beam finite element model for tapered thin-walled open cross sections beams. *Engineering Structures, 99,* 132–148.

Pavazza, R. (2002). On the load distribution of thin-walled beams subjected to bending with respect to the cross-section distortion. *International Journal of Mechanical Sciences, 44,* 423–442.

Pavazza, R., & Matokovic, A. (2000). On the shear flow due to distortion of hull cross- sections of tankers with two longitudinal bulkheads. In *Proceedings, IMAM 2000* (Vol. II, pp. F32–F39). Ischia, Italy.

Rasmussen, K. J. R. (2000). The development of an Australian standard for stainless steel structures. In *Proceedings of 15th international specialty conference on cold formed steel structures* (pp 309–338). St. Louis (MO).

Rhodes, J. (2002). Buckling of thin plates and members—and early work on rectangular tubes. *Thin-Walled Structures, 40*(2), 87–108.

Rondal, J., Wurker, K. G., Dutta, D., Wardenier, J., & Yeomans, N. (1992). *Structural stability of hollow sections*. Koln: Verlag TUV Rheinland Gmbh.

Saoula, A., Meftah, S. A., Mohri, F., & Daya, E. M. (2016). Lateral buckling of box beam elements under combined axial and bending loads. *Journal of Constructional Steel Research, 116,* 141–155.

Skaloud, M., & Naprstek, J. (1977). Limit state of compressed thin-walled steel columns with regard to the interaction between column and plate buckling. In *Proceedings of second international colloquium on the stability of steel structures* (pp. 405–414). Liege: University of Liege.

Vensson, S. E., & Croll, J. G. A. (1975). Interaction between local and overall buckling. *International Journal of Mechanical Sciences, 17,* 307–321.

Zhao, X. L., & Grzebieta, R. H. (2000). Strength and ductility of concrete filled double skin square hollow sections. In X. L. Zhao & R. H. Grzebieta (Eds.), *Structural failure and plasticity*. Rolla: University of Missouri-Rolla.